

¹ Departament d'Astronomia i Meteorologia, Universitat de Barcelona, Barcelona, Spain

² Facultad de Ciencias de Ourense, Universidad de Vigo, Ourense, Spain

³ University of Lisbon, CGUL, IDL, Lisbon, Portugal

⁴ Departamento de CC Ambientales, Universidad Pablo de Olavide de Sevilla, Sevilla, Spain

⁵ Departamento de Física de la Tierra, Astronomía y Astrofísica, Facultad de Físicas,
Universidad Complutense de Madrid, Ciudad Universitaria, Madrid, Spain

⁶ Departamento de Física, Universidad de Extremadura, Badajoz, Spain

Cloud cover analysis associated to cut-off low-pressure systems over Europe using Meteosat Imagery

G. Delgado¹, A. Redaño¹, J. Lorente¹, R. Nieto^{2,3}, L. Gimeno^{2,3}, P. Ribera⁴,
D. Barriopedro⁵, R. García-Herrera⁵, and A. Serrano⁶

With 13 Figures

Received December 21, 2005; revised March 7, 2006; accepted June 27, 2006

Published online: December 20, 2006 © Springer-Verlag 2006

Summary

This paper reports a cloud cover analysis of cut-off low pressure systems (COL) using a pattern recognition method applied to IR and VIS bispectral histograms. 35 COL occurrences were studied over five years (1994–1998). Five cloud types were identified in COLs, of which high clouds (HCC) and deep convective clouds (DCC) were found to be the most relevant to characterize COL systems, though not the most numerous.

Cloud cover in a COL is highly dependent on its stage of development, but a higher percentage of cloud cover is always present in the frontal zone, attributable due to higher amounts of high and deep convective clouds. These general characteristics are most marked during the first stage (when the amplitude of the geopotential wave increases) and second stage (characterized by the development of a cold upper level low), closed cyclonic circulation minimizing differences between rearward and frontal zones during the third stage. The probability of heavy rains during this stage decreases considerably. The centres of mass of high and deep convective clouds move towards the COL-axis centre during COL evolution.

1. Introduction

COLs are closed cyclonically circulating eddies isolated from the main westerly stream. Colder

air can be found in the upper level low than in the surrounding upper and mid-levels of the troposphere. COLs can be clearly visualized as close geopotential height contours with cold core. The troposphere below COLs is unstable and convective severe events can occur covering large areas. According to García-Herrera et al (2001) and Llasat (1991) COLs are responsible for the most important flooding episodes and catastrophic weather events in southern Europe. An understanding of the characteristics of the cloud cover associated with COL systems can improve estimations of their capacity to produce heavy rainfall and diagnostics of their development and evolution. Numerous previous works focus on the importance of COLs in mechanisms of stratosphere-troposphere exchange (Bamber et al, 1984; Holton et al, 1995). Hoskins et al (1985) and Wirth (1995) presents other mechanism of stratosphere-troposphere exchange: turbulent mixing near the jet stream associated with the COLs and tropo-pause folding along the system. Gimeno et al (1998) focus on the stratosphere-troposphere

exchange to explain anomalous values of tropospheric ozone. Other authors present climatological studies of COLs in the Northern Hemisphere (Hernández, 1999; Kentarchos and Davies, 1998; Price and Vaughan, 1992). Finally, Krennert and Zwatz-Meise (2002) presents a subjective characterization of COLs systems using satellite imagery as a simple visual guide to identify these systems in the images.

This study presents a cloud cover analysis of COLs, using a cloud classification algorithm involving the computation of some parameters describing the spatial distribution of the clouds, their textural appearance and their potential to produce heavy rainfall. Most studies related to cloud classification focus on improving the pattern recognition method (Arking and Childs, 1985; Desbois et al, 1982; England and Hunt, 1985; Massons et al, 1996) and it is not common to use this as a tool to analyze or describe a COL phenomenon. In other cases the method is used to study certain events or to obtain seasonal cloud cover cycle estimates (Massons et al, 1998).

Several statistical cloud classification methods have been tested in recent year (Pankiewicz, 1995; Porcú and Levizzani, 1992; Rossow and Garder, 1993; Sèze and Desbois, 1987). The algorithms used in some of these studies are based on the k-means method. Pattern recognition is conducted on the VIS-IR bispectral histogram and it is necessary to specify the final number of cloud types due to the difficulty of obtaining stable training areas. The complexity of the image suggested to us the use of unsupervised classifiers (Massons et al, 1996). The accuracy of this method has been demonstrated, although it still presents some problems with low-contrast situations in the imagery.

This study is part of a research project, Validación Climática de Modelos Conceptuales a Escala Sinóptica (VALIMOD), whose objectives include the analysis and validation of COL systems using the NCAR-NCEP reanalysis data and METEOSAT images. Climatology was constructed using 41 years (1958–1998) of NCAR-NCEP reanalysis data (Nieto et al, 2005) for the Northern Hemisphere. There are three preferred areas of COL occurrence: Southern Europe and the eastern Atlantic coast, the eastern North Pacific coast and the north eastern United States and North China-Siberian region, extending to north

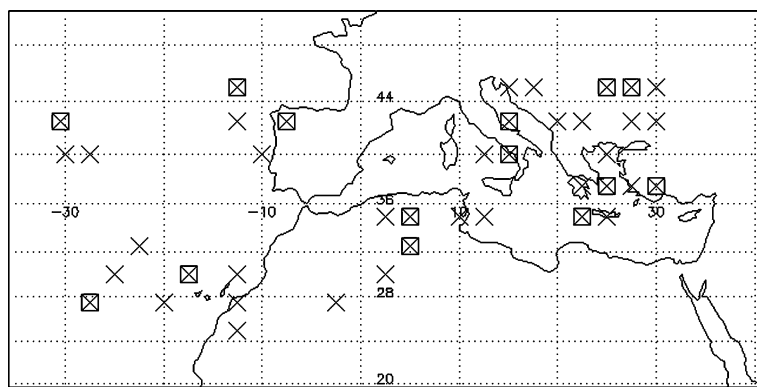
western Pacific coast. The European area was chosen as it is one of the regions where COLs are most common (Price and Vaughan, 1992; Kentarchos and Davies, 1998), and it is the area covered by the METEOSAT satellite. This paper presents the results obtained from cloud cover analysis of COL occurrence over five years (1994–1998). Some statistics concerning cloud types and their distribution in the COL selected area using the VIS and IR METEOSAT channels were obtained in order to characterize the cloudiness of this synoptic atmospheric system.

2. Methodology

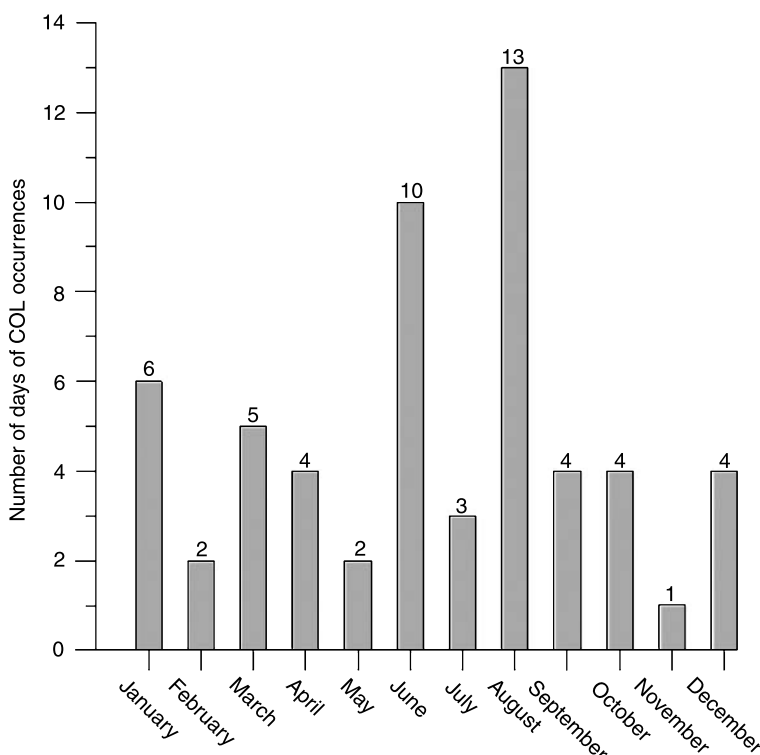
COL systems are closed cyclonically circulating eddies isolated from the main western stream. These lows are upper and mid-tropospheric dynamic structures and they do not tend to spread to lower levels of the troposphere. Air within a COL is colder than in the surroundings. The typical life cycle of a COL can be separated into four stages: upper level trough, tear-off, cut-off and the dissipation stage (Krennert and Zwatz-Meise, 2002). During the first stage, significant cold air advection occurs and the amplitude of the geopotential wave increases. The tear-off stage is characterized by the development of a cold upper level low within the southern part of the trough. During the third stage, the upper level trough is cut-off and becomes a separate upper level low, showing closed cyclonic circulation. The upper level low usually merges with a large upper trough in the main zonal flow during the dissipation stage.

The images processed in this paper are from METEOSAT 7 at 12 UTC and have a peak spatial resolution of 5 km (IR and WV) and 2.5 km (VIS) at the subsatellite point. COL systems northward of 45° or southward of 25° and eastward of -30° or westward of 30° were not included in the study in order to avoid large viewing angles which would give erroneous results due to the satellite projection used. Figure 1a shows the domain chosen for this study and Fig. 1b the monthly distribution of days of COL occurrences.

35 COL occurrences are analyzed in this study. Although more COL occurrences were detected in Nieto et al (2005) during the period studied, a large part of the METEOSAT images was damaged, which made the selection of the area



a



b

Fig. 1. Distribution of all the days analyzed over 5 years (a). Square symbols indicate that two or more days of COL occurrences were located in that position. Monthly distribution of all the days analyzed (b)

of study of some of the days difficult. 35 COL occurrences (involving 58 days) were found to be a significant sample for the statistical purposes. Most of the COL occurrences detected in Nieto et al (2005) last 2–3 days. Due to the problems with some of the images not in all the cases were possible to analyze the whole COL occurrence; consequently 14 of the COL occurrences were analyzed using one day. The rest of the cases were studied using the total days they last: 2 days in 19 COL occurrences and 3 days in 2 COL occurrences. Twelve of the images used were from 1994, 17 from 1995, 5 from 1996, 8 from 1997 and 16 from 1998. Figure 1 shows

the distribution of the COL occurrences analyzed in this paper.

2.1 Cloud classification

IR-VIS bispectral histograms obtained from visible and infrared (Fig. 2) grey values were submitted to a cluster analysis. The grey level counts are inverted for IR channel; therefore, low IR values correspond with high brightness temperature. A low pass filter is applied to the bispectral histograms in order to reduce spurious peaks (Massons et al, 1996). The basis of the algorithm presented in this paper has been developed by

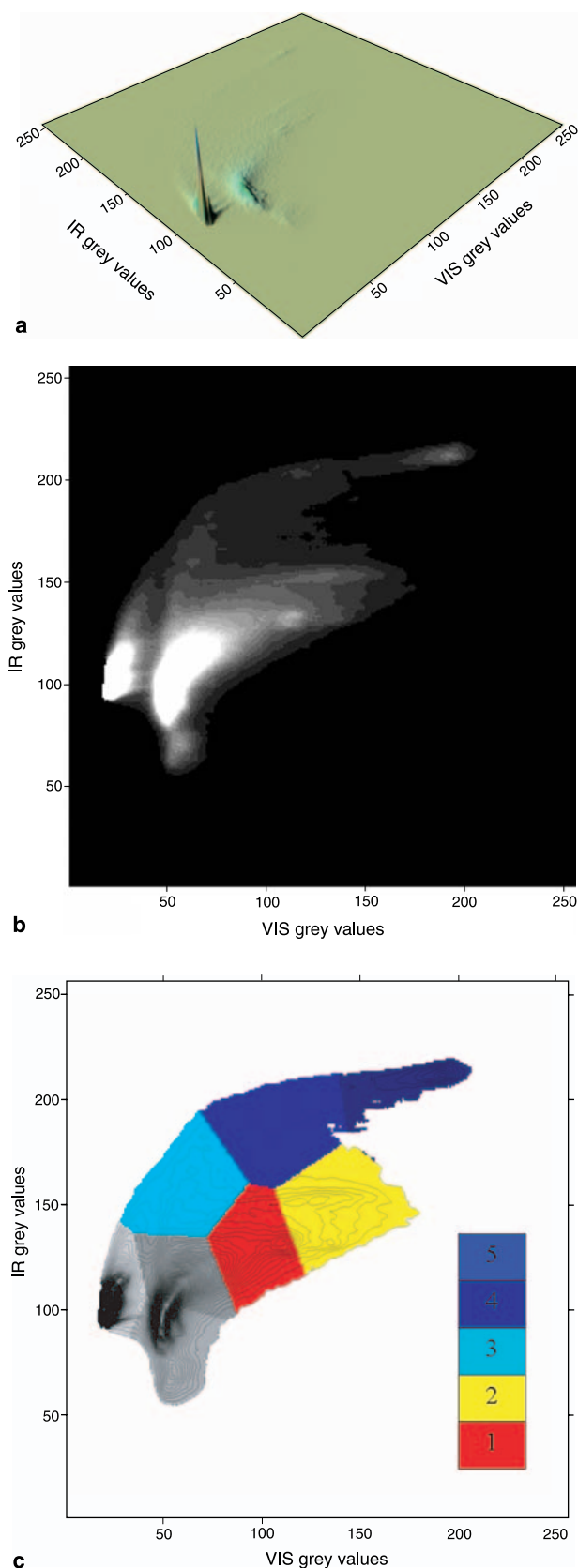
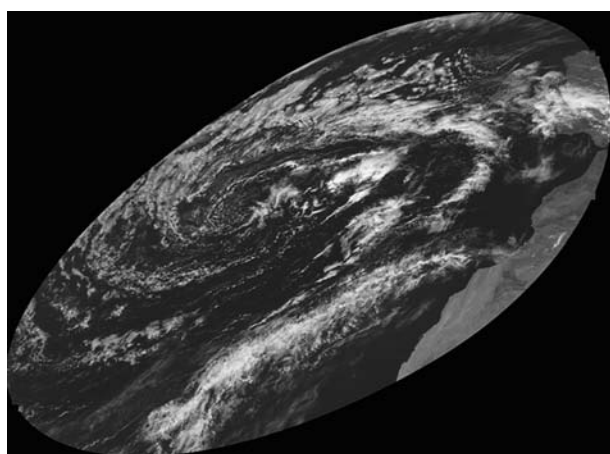


Fig. 2. Bispectral histogram in a 3D (a) and 2D (b) representation and classified results: Dark blue (C5), blue (C4), light blue (C3), yellow (C2) and red (C1) (c). The region of grey colour corresponds to land and sea

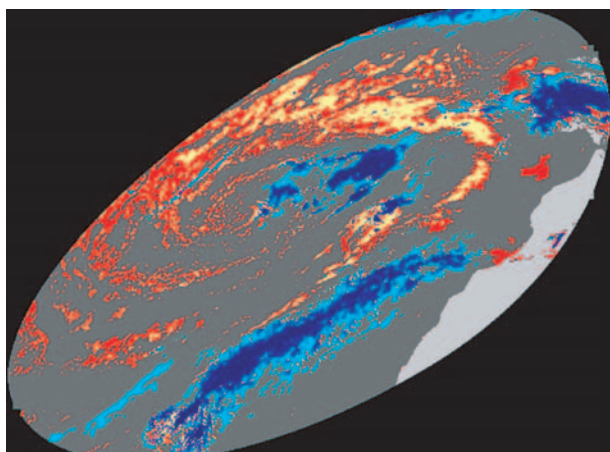
Porcú and Levizzani (1992) and Massons et al (1996). Each point in the bispectral histogram has an IR coordinate and a VIS coordinate. The value of the point corresponds to the number of pixels with these IR-VIS grey values in both channels. All the local maximums (from 800 to 1000 approximately, depending on the image) in the IR-VIS bispectral histogram are located by the algorithm in the first step. Starting from this initial partition, each point in the bispectral histogram is assigned to the nearest local maximum and flagged in a class, thus the initial number of local maximums gives the initial number of classes. The algorithm is iterative: a different partition of the bispectral histogram is generated after each step. A pixel is classified in one class or another depending on its position in the bispectral histogram, using the Euclidean distance as clustering technique classifier. Two variables are considered in determining whether one class should be rejected in favour of another: the number of elements of in the class and the distance between the two classes. The method requires an exact specification of the final number of classes, thus both conditions were modified in each case in order to obtain one or two land areas, one sea surface and five cloud types. It is found that the optimal number of classes is seven or eight. Depending on the latitude studied, the image can have two different land types; one being colder than the other. This is observed in those areas including Europe and North-Africa. Any other partition would produce classes without physical meaning. The final distribution of the classes in the bispectral histogram is slightly different depending on the image; this is due to the different cloud distribution. These little differences do not affect the quality of the classification. This means that pixels classified as deep convective clouds in different images have always the greater IR-VIS values. Clouds were classified as follows: Low clouds (C1), mid/thick clouds (C2), mid/thin clouds (C3), high clouds (C4) and deep convective clouds (C5). Figure 2 shows the classification on the bispectral histogram. Low clouds were often classified as land or sea surface areas, the optimal selection of the minimum distance between classes and the minimum elements belonging to a class helped avoid this problem. Using two classes of mid clouds permits to choose an optimal number of final classes, which is primordial in obtaining

a correct classification. In case of absence of any of the cloud types in a given case 4 classes of clouds were have been the final number of classes chosen.

Class C1, with low IR values (high brightness temperature), is associated with mist, stratus and cumulus humilis. Class C2, with high VIS values and IR values greater than class 1, is associated with altocumulus/cumulus and nimbostratus. Class C3, with low VIS values and mid-high IR values, is associated to altostratus. Class C4, with high IR values, is associated with cirrus, cirrocumulus and cirrostratus, and C5 is associated with cumulonimbus with high IR and VIS values. Figure 3 shows an example of the cloud classification made for an image of the eastern Atlantic region.



a



b

Fig. 3. VIS Image 16-06-95 at 12:00 UTC showing the eastern Atlantic area (a) and classification into five cloud classes (b). High and deep convective clouds are represented in dark blue and blue color, respectively

2.2 Area associated with a COL

The climatology developed by Nieto et al (2005), relates each COL system to a corresponding grid point of the NCAR-NCEP reanalysis files. The area selected to analyze the cloudiness associated with a COL needs to cover the region influenced by the synoptic structure. Although geopotential height at 300 hPa is usually used over midlatitudes, the identification of COL occurrences done by Nieto et al (in which is based this paper) was done using geopotential height at 200 hPa. For this reason height contours of 200 hPa (from NCAR-NCEP reanalysis data) are superimposed onto the VIS image of the satellite in order to demarcate the area of study associated with each COL system. Figure 4 shows a COL in the first stage with a well formed upper level trough and associated cloudiness distributed along the height contours. In order not to include cloud systems not associated with the COL studied, the image was cut out following an asymmetric ellipse form with four different axes. The same figure shows the new selected area. The center of the asymmetric ellipse has the same latitude and longitude than the identification of each COL occurrence done by Nieto et al. The identification is carried out imposing three consecutive conditions to the 200 hPa geopotential height: geopotential minimum and cutoff circulation, equivalent thickness difference between 200 and 300 hPa and the thermal front parameter. The orientation of the ellipse is decided depending on the case in order to select the appropriate area of study. The

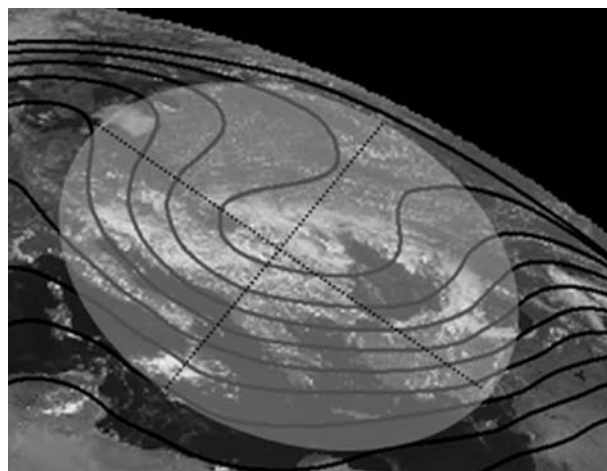


Fig. 4. VIS Image 18-08-96 at 12:00 UTC, showing the demarcation of the selected area of study. The asymmetric ellipse axes are represented in dotted lines

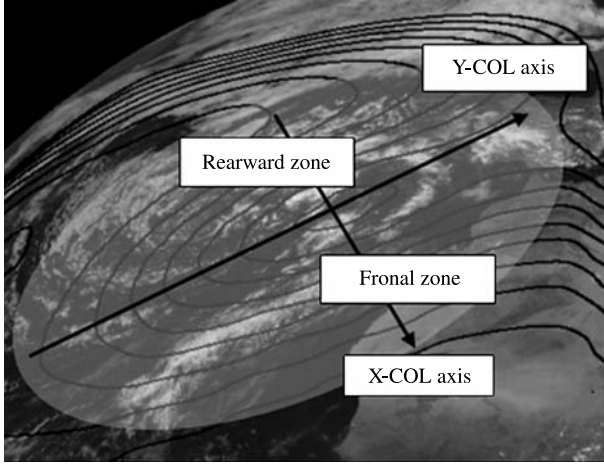


Fig. 5. VIS Image 16-06-95 at 12:00 UTC, showing the COL-axes system. The Y-COL-axis divides the entire area in two regions: the rearward and the frontal zone. In this case COL-axes system coincides with the asymmetric ellipse axes

dissipation stage is characterized by the restitution of the general circulation following the mean zonal flow, in which no specific pattern in spatial cloud distribution is expected to be found, for this reason it has not been analyzed.

Figure 5 shows another COL system in the second stage. The system has been divided into two different zones in order to analyze the evolution and distribution of cloudiness: the front of the COL, or leading zone, is upstream of the 200 hPa trough axis region and the rear of the COL, or rearward zone, is downstream of this region.

2.3 Parameters used in the characterization of COLs

COL-axes: The Y-COL is the 200 hPa trough axis. Sometimes the orientation of this axis coincides with the orientation of the asymmetric ellipse used to select the area of study, but this is not always the case. The X-COL axis is perpendicular to the Y-COL axis. Figure 5 shows the COL-axes system.

Cloud area (CA) is the number of pixels covered by a cloud type within the asymmetric ellipse.

Percentages of the cloudy area: Two percentages were calculated for each cloud type: the area of the cloud type divided by the whole selected COL area (WCA) and the area of the cloud

type divided by the total cloudy area (CCA) within the whole selected COL area. Both percentages give similar information.

Mean IR and VIS brightness count (MIR, MVIS): The mean IR and VIS brightness grey values of each cloud type were calculated using the formulae $\Sigma bc_{(IR)i}/N$ and $\Sigma bc_{(VIS)i}/N$, respectively, where $bc_{(IR)i}$ and $bc_{(VIS)i}$ are the brightness count of pixel i of the cloud type in the IR and VIS channel and N is the total number of cloud type pixels (Feidas and Cartalis, 2001).

Coordinates of the centre of gravity (X_C, Y_C): This parameter is calculated using the following formulae:

$$X_C = \frac{\sum (bc_{(IR)i} + bc_{(VIS)i})x_i}{\sum (bc_{(IR)i} + bc_{(VIS)i})},$$

$$Y_C = \frac{\sum (bc_{(IR)i} + bc_{(VIS)i})y_i}{\sum (bc_{(IR)i} + bc_{(VIS)i})}, \quad (1)$$

where x_i and y_i are the coordinates of the cloud pixel in the image (Feidas and Cartalis, 2001).

Normalized distance (ND) is defined as the distance between the centre of gravity of each cloud type and the centre of the COL-axes system divided by the distance between the centre of the COL-axes system and the farthest point of the defined COL area in the direction defined by the line connecting the centre of the COL-system axis to the centre of gravity of the cloud type. The normalized distance can be greater or equal to zero and is less than or equal to one. Normalized distance will be one within the limit of the defined COL area.

Texture index (TI) is calculated using the Sobel operator. The Sobel operator is a nonlinear edge filter, which describes the local variability of the grey edge fields. The Sobel value associated to a pixel (p_{ij}) is given by

$$S = \sqrt{S_x(p_{ij})^2 + S_y(p_{ij})^2}, \quad (2)$$

where S_x and S_y are the partial derivatives:

$$S_x = \begin{pmatrix} -1 & 0 & 1 \\ -2 & 0 & 2 \\ -1 & 0 & 1 \end{pmatrix}, S_y = \begin{pmatrix} -1 & -2 & -1 \\ 0 & 0 & 0 \\ 1 & 2 & 1 \end{pmatrix}. \quad (3)$$

These mathematical operators are applied to the first neighbors of the pixel.

The Sobel operator is used to describe the local texture of patterns seen in VIS images. Values of the Sobel operator applied to HCC top are larger than the values associated with land area which is also smoother. The Sobel value associated with a class is the mean value over all the pixels of the class.

Volume index of a class (VI) is defined as (Arnaud et al, 1992),

$$VI = \sum n_i(bc_i - bc_o), \quad (4)$$

where n_i is the number of pixels with the same brightness count bc_i and bc_o is the minimum brightness count value belonging to a class. In this study, volume index is the average value of three volume indices for IR, VIS and WV bands, following the definition in Feidas and Cartalis. The VI index for deep convective clouds, is a measure of the potential of the cloud to produce heavy rainfall (Feidas and Cartalis, 2005). The mean values of bc_o to compute the VI for DCC are:

$$bc_{o(IR)} = 170 \pm 12 \quad bc_{o(VIS)} = 123 \pm 26,$$

$$bc_{o(WV)} = 164 \pm 17.$$

3. Results and discussion

The cloud classification algorithm was applied to midday images corresponding to 35 COL cases. The main results of the cloudiness characterization of COL systems are following.

3.1 Percentage of cloudiness

Percentages of the area of COL systems covered by each class of cloud (WCA) were calculated for

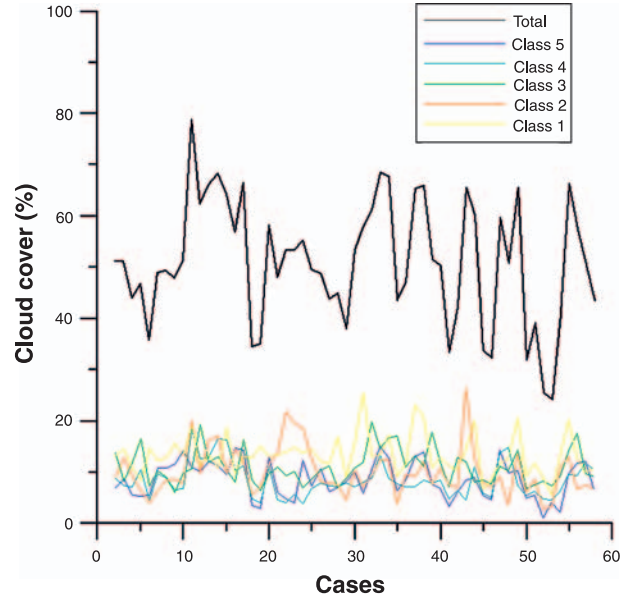


Fig. 6. Averaged values of whole cloud area (WCA) in the COL selected area for each studied cases. Red colour represents low clouds and yellow mid-level clouds

each case (Fig. 6). The contribution of each class to the total area and to frontal and rearward zones was estimated computing the average of cloud cover for every cloud type over all the cases of COL occurrence analyzed. Table 1 summarizes these contributions. WCA, RWCA, FWCA are the averages of the percentage of presence of each cloud type in the whole COL area, in the rearward region and in the frontal region respectively. It is clear that mid and low clouds (C1, C2 and C3) contribute to the total cloudiness more than high and deep convective clouds (C4 and C5). Nevertheless COL are synoptic systems localised in the upper and mid troposphere whose formation is related with the general circulation,

Table 1. Average values of the percentage of presence of each cloud type in the whole COL selected area (WCA), in the rearward region (RWCA) and in the frontal region (FWCA). Average values of the percentage of presence in the cloudy area within the COL selected area (CCA), the rearward region (RCCA) and the frontal region (FCCA) for each cloud types. Percentages of low and mid clouds are greater than high and deep convective clouds in the whole COL selected area. Nevertheless the contribution of high and deep convective clouds in the frontal zone is higher than low and mid-level clouds

%	C1	σ_1	C2	σ_2	C3	σ_3	C4	σ_4	C5	σ_5	Total	σ_T
WCA	13.31	3.95	9.99	4.79	10.92	3.44	8.28	3.38	8.45	3.60	50.94	12.12
RWCA	14.73	5.63	12.14	9.26	9.87	5.28	4.96	3.31	4.79	2.75	42.93	14.50
FWCA	12.62	6.18	9.02	4.56	11.58	4.09	10.28	5.63	10.89	4.25	54.40	17.36
CCA	26.53	6.38	19.26	6.96	21.85	5.92	16.19	4.58	16.17	5.09	100	
RCCA	33.11	12.49	24.69	12.91	22.14	11.41	10.55	5.75	9.51	4.30	100	
FCCA	23.61	9.24	16.18	6.87	22.28	7.34	18.63	6.33	19.30	6.83	100	

thus low and mid-level clouds do not seem the more appropriated to characterize COL's systems. To determine what cloud types are most characteristic of COL systems, rather than simply most numerous, further analyzes are required. The formation of low and mid/thick clouds over land is in most cases related with mesoscale dynamics and determined by orography. This is clear in the case of Lee cloudiness and Stau cloudiness (Krennert and Zwatz-Meise, 2002). So, C1 and C2 cloudiness formation during COL occurrence is a consequence of the interaction between mesoscale and synoptic scales, accelerated by orography when over land. Therefore, although they contribute highly (see Table 1) to total cloudiness, low and mid clouds do not seem suitable in characterising COL systems and their evolution. Table 2 summarizes the correlation coefficients between the percentages of each type of cloud for the whole area and for rearward and frontal zones. The correlation between C4 and C5 classes is the strongest. It is clear, therefore, that high cloud formation can be related with deep convective cloud formation and, therefore, that C4 and C5 cloud formation and evolution is linked with the COL life cycle. This becomes obvious if we pay attention to the correlation coefficients between these classes for the rearward and frontal zones separately (Table 2). This is the only case where correlations are higher within each zone than in the overall area. Thus, the appearance and distribution of high convective clouds seems to respect

Table 2. Correlation coefficients between the percentages of cloud cover of each class for the whole COL selected area and the rearward and frontal zones separately. High and deep convective clouds are more correlated in both frontal and rearward zone than in the whole COL selected area

	Total area	Rearward zone	Frontal zone
r_{12}	0.329	0.292	0.261
r_{13}	0.074	0.318	-0.197
r_{14}	0.137	-0.053	-0.084
r_{15}	0.295	-0.060	0.099
r_{23}	0.060	0.130	-0.144
r_{24}	0.119	0.260	-0.109
r_{25}	0.274	0.452	0.037
r_{34}	0.350	0.419	0.327
r_{35}	0.315	0.306	-0.008
r_{45}	0.560	0.691	0.675

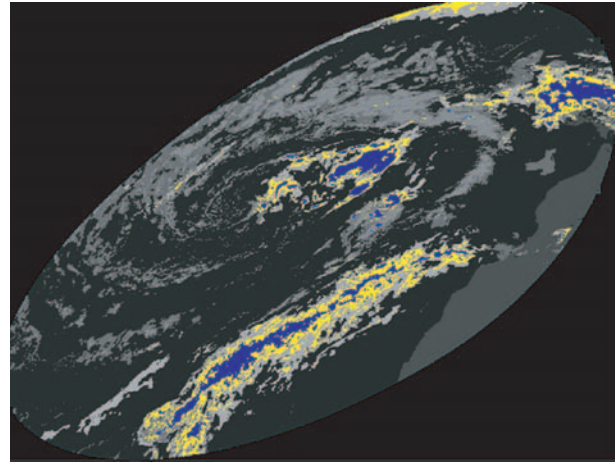


Fig. 7. VIS Image 16-06-95 at 12:00 UTC showing high clouds (in yellow) and deep convection clouds (in blue). The high correlation between these types of clouds is clear in this figure

the division of the COL into rearward and frontal zones, as described in the methodology. A consequence of this is that C4 clouds are associated with the anvils of cumulonimbus clouds of class C5 (Fig. 7).

Therefore, high and deep convective clouds seem to be the classes that best characterize the COL system life cycle. Table 1 shows that, on average, half of the total COL area is covered by

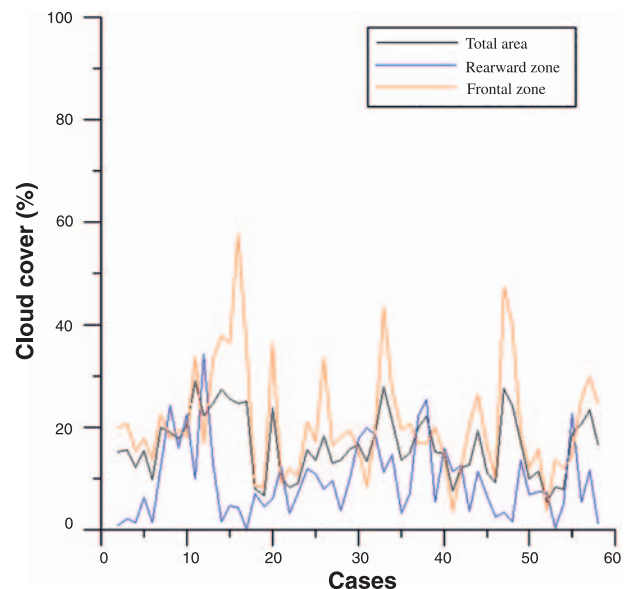


Fig. 8. Averaged values of WCA, RWCA and FWCA for high and deep convective clouds for each studied cases. High and deep convective clouds has a major presence in the frontal zone of the COL selected area

Table 3. Average values of the percentages WCA, RWCA and FWCA for each stage. The apparition of convection in the frontal zone increases during the second stage and drops during the third

%	C1	σ_1	C2	σ_2	C3	σ_3	C4	σ_4	C5	σ_5	Total	σ_T
Stage 1												
WCA	12.85	4.88	9.93	5.87	10.95	2.87	7.92	3.42	7.55	3.28	49.20	11.13
RWCA	14.75	6.14	12.40	7.68	10.99	5.31	5.04	2.60	4.19	2.47	47.37	15.04
FWCA	11.43	5.52	9.45	4.85	10.77	2.46	9.41	3.65	9.92	3.15	50.98	12.81
Stage 2												
WCA	13.41	3.73	10.30	4.58	10.92	3.99	8.30	3.40	9.04	3.84	51.97	9.28
RWCA	15.06	4.69	12.06	5.51	9.21	3.27	4.06	1.49	4.26	1.12	44.66	12.10
FWCA	12.97	3.96	9.34	4.26	12.02	4.52	10.82	3.58	12.10	4.05	57.26	12.99
Stage 3												
WCA	13.69	3.20	9.57	3.86	10.89	3.33	8.67	3.48	8.59	3.61	51.41	8.02
RWCA	14.19	5.22	11.96	6.45	9.60	3.90	6.31	2.26	6.35	2.15	48.41	11.26
FWCA	13.50	5.77	7.97	3.20	11.85	4.9	10.48	2.94	10.13	3.00	53.93	12.78

clouds. Cloudiness in the frontal zone is higher than in the rearward zone due to the contribution of C4 and C5 clouds. Approximately 11% of the frontal zone is covered by these types of clouds and only a 5% is covered in the rearward zone. Other cloud types do not seem to follow this pattern. As has been discussed before C4 and C5 seem to describe COL evolution better than low and mid clouds, despite being less significant quantitatively. Figure 8 shows the different percentages of C4 and C5 clouds between zones for each COL occurrences.

CCA, RCCA and FCCA in Table 1 are the averages of the percentages of each cloud type in the whole cloudy area, in the rearward zone cloudy area and in the frontal zone cloudy area, respectively. The same differences between zones can be seen.

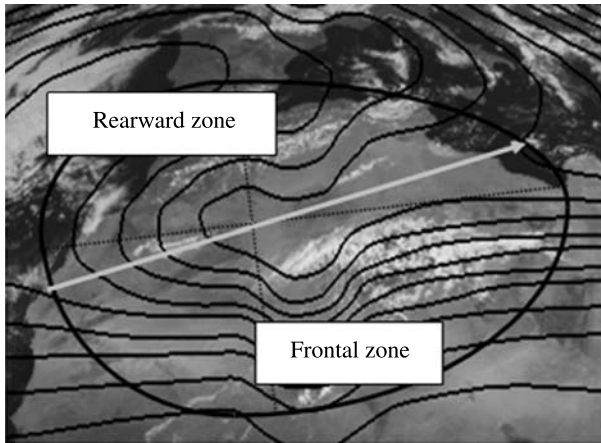
Table 3 summarizes the same statistics for each of the stages of the COL life cycle. The upper level trough stage is characterized by cloudiness similar to the average for all stages: that is to say, cloud cover is about 50%, rising in the frontal zone on account of the high cloud distribution. The tear-off stage is characterized by an increase of cloudiness in the frontal zone, as a result of increasing convection from the first to the second stage. The cut-off stage follows the same pattern, but with increasing cloudiness in the rearward zone due to closed cyclonic circulation. Figure 9 shows changes in cloudiness distribution between the first and second stages. Closed cyclonic circulation during the third stage is shown in Fig. 10. The same calculations have

been made for COL occurrences during the warm season (April–September) and the cold season (October–March). Few differences can be detected, though the difference between rearward and frontal zone seems to be accentuated during the cold season.

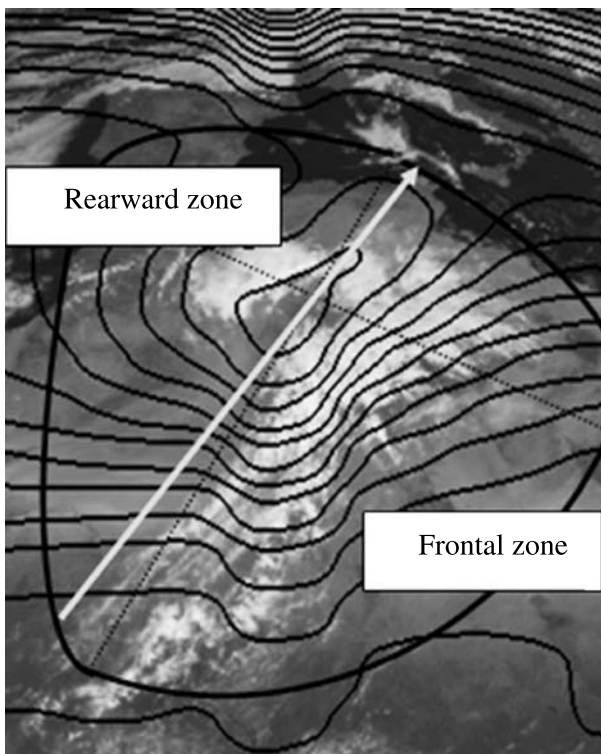
3.2 Spatial distribution

Four quadrants have been defined in the COL area: the first one comprises the region between the positive Y-COL axis and positive X-COL axis and corresponds to the upper side of the frontal zone. The second and third quadrants correspond to the upper and lower side of the rearward zone respectively and the fourth quadrant is the lower side of the frontal zone. Table 4 shows the percentage of the presence of mass centres of C4 and C5 classes in every quadrant for each case and each stage. High and deep convective cloud tends to be present in the upper side of the frontal zone. Naturally, clouds are spread out across the whole COL area but the presence in the upper frontal zone is more important than other ones (Table 4). This pattern is illustrated in Fig. 11.

The evolution of the position of the mass centres of C4 and C5 cloud classes during the different stages (Table 4) in the quadrants defined before show that the upper side of the frontal zone is clearly the most populated during the three stages. This situation is very clear during the first stage becoming more moderate during the second. Closed cyclonic circulation during the third stage tends to distribute HCC across the four quadrants.



a



b

Fig. 9. VIS Image 14-03-94 (a) and 15-03-94 (b) at 12:00 UTC showing the evolution of cloudiness from the first (a) to the second stage (b). In these cases the COL system axes does not coincide with asymmetric ellipse axes (dotted lines)

The normalized distances (ND) of the centres of mass over all cases of COL occurrence and for every stage computed for each cloud type is presented in Table 5. Low and mid clouds are found closer to the origin of COL-axes systems than high and deep convective clouds. These are situated on average at a normalized distance (ND) equal to 0.5 (in the middle region of the COL selected area).

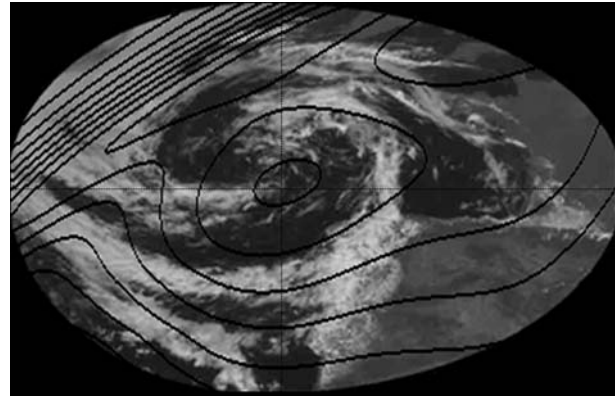


Fig. 10. VIS Image 04-08-95 at 12:00 UTC showing closed cyclonic circulation during the third stage of a COL-system

Table 4. Percentage of the number of mass centres of high and deep convective clouds in every quadrant over all cases, for each stage. Convection is more likely to appear in the first quadrant (delimited by the positive COL-axes in the upper side of the frontal zone). This tendency decreases in the second and third stages in favor of the fourth quadrant (in lower side of the frontal zone)

%	1st quadrant	2nd quadrant	3rd quadrant	4th quadrant
Total	51.75	18.42	10.53	19.30
Stage 1	66.67	19.44	2.78	11.11
Stage 2	52.08	14.58	16.67	16.67
Stage 3	36.67	23.33	6.67	33.33

Table 5 also presents the spatial evolution of the mass centres during the different stages of the COLs. The mass centres of C4 and C5 cloud classes tend to move towards the centre of the COL-axes system over the life cycle; this behavior has not been observed in the case of low and mid clouds.

In order to better understand the evolution of cloud cover in COL systems, three concentric regions inside COL area were defined. The first one includes pixels that lie between the COL-axes system centre and 1/3 of ND (region 1). The second one comprises pixels that lie between 1/3ND and 2/3ND (region 2). Finally, the third region takes in pixels that lie between 2/3ND and ND (region 3). Table 6 summarizes the percentage of gravity centres of each class for every region and stages across all days of COL occurrence. Overall, but particularly in the first stage, C4 and C5 clouds are concentrated in region 2 with less presence region 1. Region 3 (near the

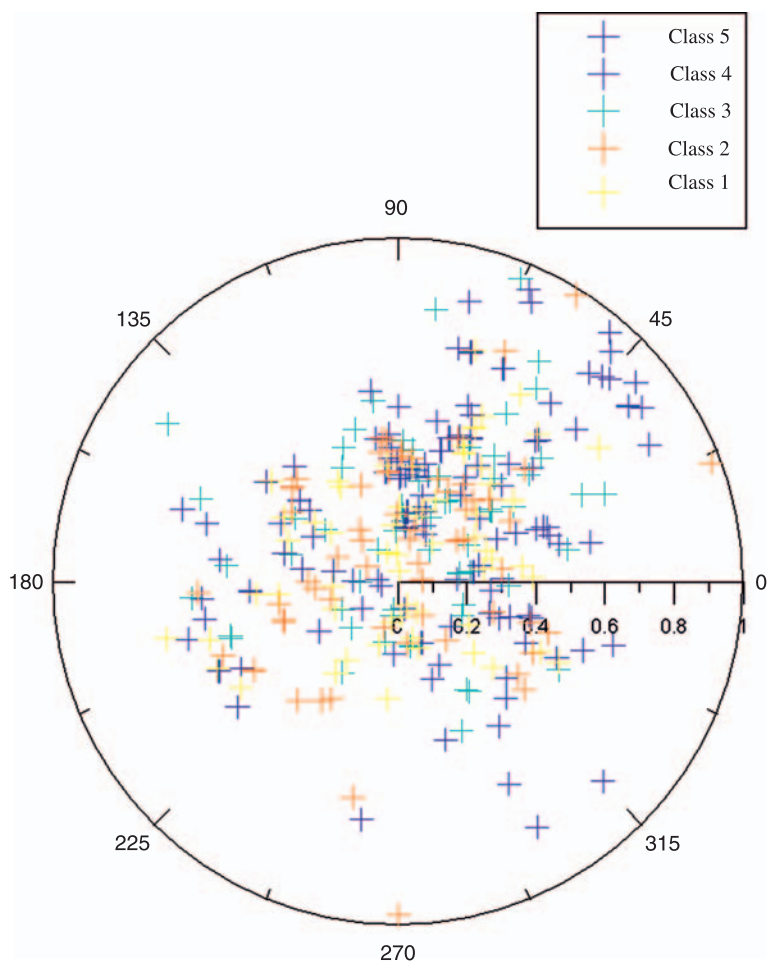


Fig. 11. Distributions of the centre of mass of each class in the COL selected area for each studied cases. Clearly the first quadrant (upper side of the frontal zone) is more likely to the apparition of convection

Table 5. Average normalized distance values for each class for each stage. Low and mid level clouds are more likely to appear closer to the center of the COL-axes system than high and deep convective clouds. This tendency decreases during COL evolution

	C1	σ_1	C2	Σ_2	C3	σ_3	C4	σ_4	C5	σ_5
ND	0.34	0.17	0.37	0.19	0.39	0.19	0.44	0.23	0.47	0.20
ND stage 1	0.35	0.15	0.30	0.12	0.37	0.17	0.49	0.20	0.51	0.23
ND stage 2	0.32	0.19	0.40	0.23	0.40	0.21	0.45	0.23	0.45	0.20
ND stage 3	0.34	0.15	0.39	0.21	0.38	0.21	0.39	0.24	0.44	0.17

limits of the COL area) is the region with the lowest percentage. Displacement to the COL-axes centre during the second stage is clear. This tendency increases during the third stage confirming the movement of high and deep convective clouds towards the COL-axes centre during the evolution of the system.

3.3 Brightness counts

The mean IR and VIS brightness count for each cloud type in every stage was determined in order

to study the radiative properties of the clouds within the COL selected area, rather than its percentage of presence and its spatial resolution. The higher pixel's IR brightness count, the colder it is. The reflectivity of a pixel is proportional to its VIS count value.

Cloud cover and IR brightness count values differences between the rearward and frontal zone was found. Thus, IR brightness values are higher in the frontal zone than in the rearward zone for C4 and C5 clouds, indicating that the tops of these cloud types are colder in the frontal

Table 6. Average of the percentages of pixels of each class in each of the three defined regions. The same calculations for each stage are presented. High and deep convective clouds seems to move towards the center of the COL-axes systems during COL evolution

	%	C1	C2	C3	C4	C5
Stage 1	Region 1	50.88	43.86	42.12	31.58	31.58
	Region 2	43.86	49.12	47.37	47.37	45.61
	Region 3	5.26	7.02	8.77	15.79	21.05
Stage 2	Region 1	33.3	66.67	44.44	22.2	16.67
	Region 2	66.67	33.33	50.00	61.11	55.56
	Region 3	0.00	0.00	5.56	16.67	27.78
Stage 3	Region 1	62.50	29.17	37.50	29.17	37.50
	Region 2	25.00	58.33	50.00	50.00	41.67
	Region 3	12.50	12.50	8.33	16.67	16.67

zone than in the rearward zone (Fig. 12); whereas similar VIS reflectivity values are obtained in both COL zones.

The same rearward-frontal pattern is observed in every of the three stages, but some differences between stages can be seen. High clouds and deep convective clouds are colder and have higher

reflectivity in the second stage than in the first one. This is consistent with the intensification of the system due to high convection in the frontal zone described in the last section. Between the second and the third stages, cloud top temperature remains constant whilst the rate of increase of reflectivity drops off.

3.4 Textural appearance

The Sobel operator has been applied to the VIS images. Once again C4 and C5 cloud class values seem to agree with COL structure defined by two zones. Rearward zone values are considerably greater than frontal zone values. This behaviour is still clearer during the first stage of COL, indicating fibrous and rough HCC in the rearward zone during the formation of the upper level trough. During the second stage, Sobel values in the frontal zone increase moderately coinciding with the appearance of convection in this zone. In the dissipation stage, rearward values of the Sobel operator decrease, minimising the difference between zones as a consequence of the homogenisation of cloudiness due to closed cyclonic circulation.

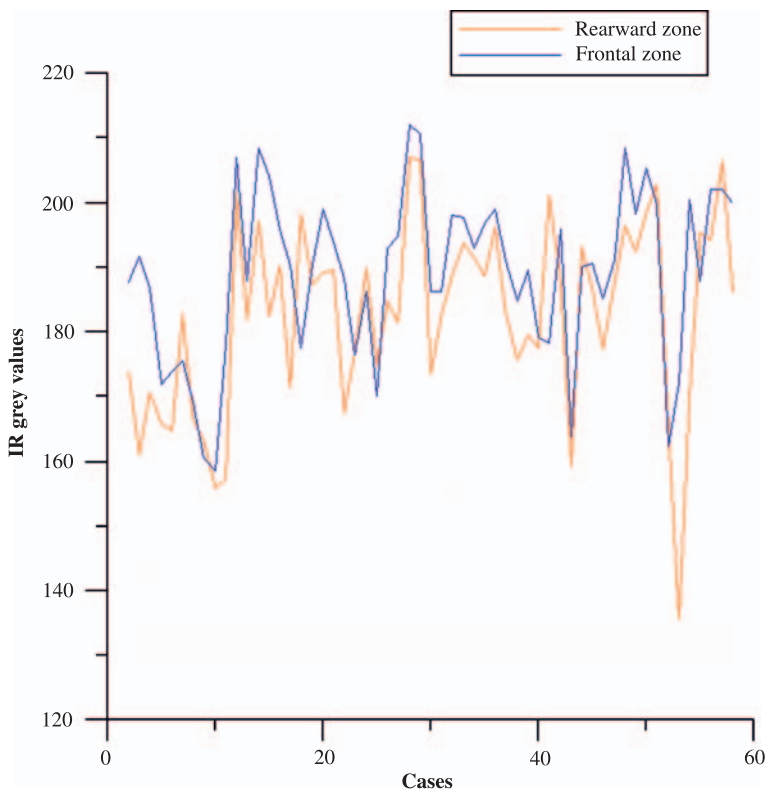


Fig. 12. Average values of IR brightness counts for the rearward and frontal zones for each studied case. Higher values in the frontal zone indicate cooling in this zone

3.5 Heavy rainfall estimation

Figure 13 shows volume index values for the C4 and C5 cloud class versus the X-COL coordinates of the centres of mass for each studied day of COL occurrence and for each stage. X-COL positive values correspond to the frontal zone and X-COL negative values correspond to the rearward zone. It

is clear that centres of mass are more frequent in the frontal zone. This pattern is also observed in Fig. 13b and c during the first and second stages. Higher activity during the second stage is also clear. During the third stage, centres of mass are uniformly distributed along the X-COL axis (Fig. 13d). To summarize, during the second stage,

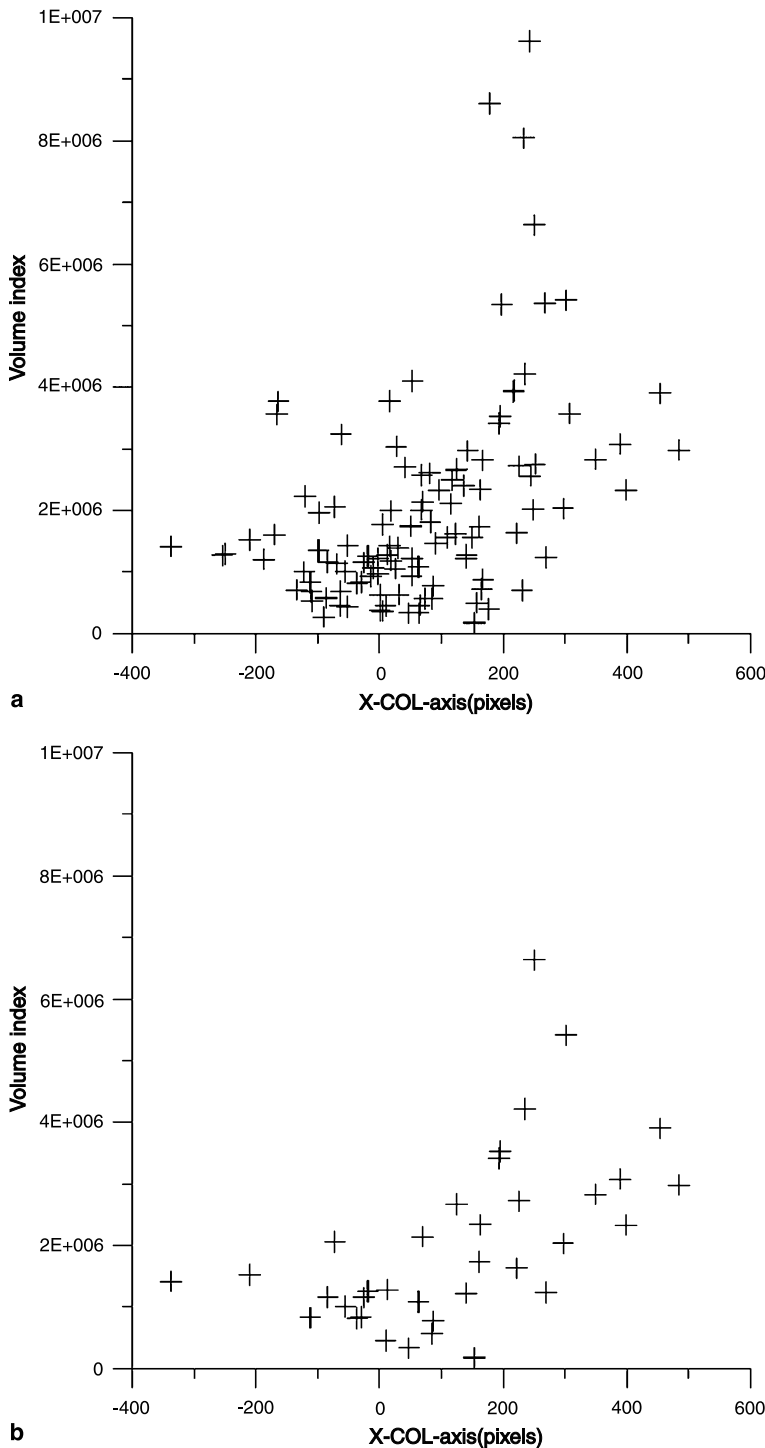
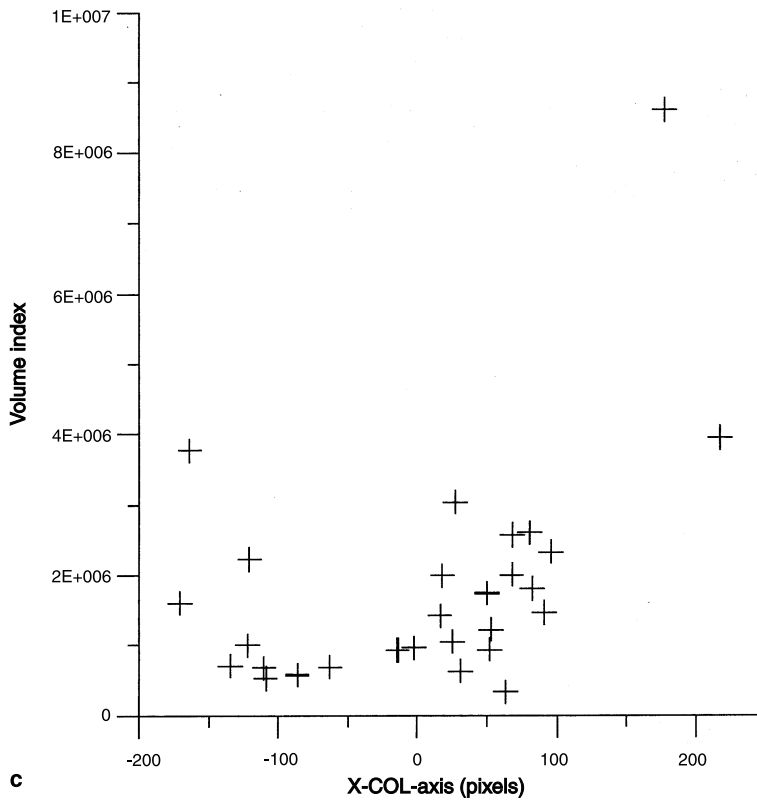
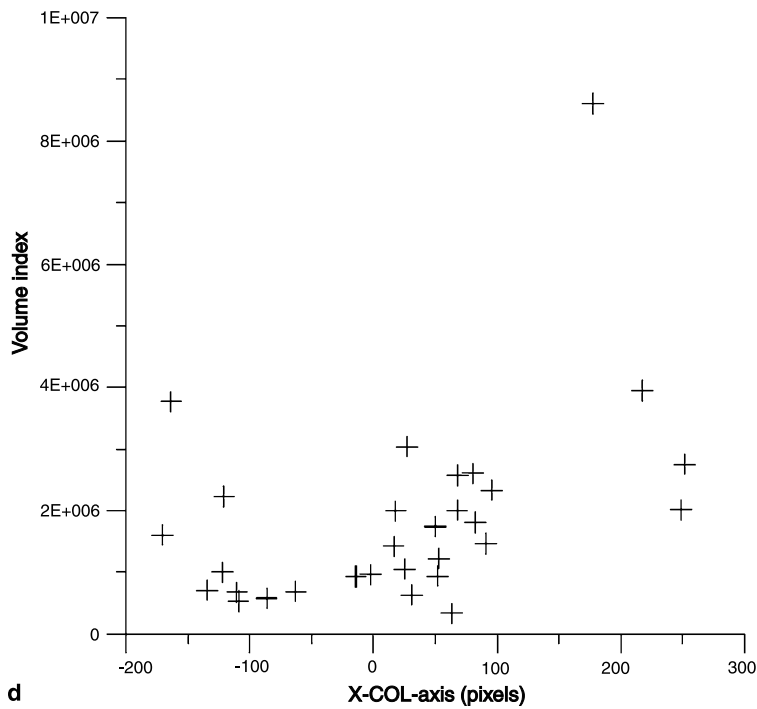


Fig. 13. Average values of the Volume index for high and deep convective clouds versus X-COL coordinates (in pixels) for each studied case (a), first stage cases (b), second stage cases (c), third stage cases (d), cold season cases (e) and hot season cases (f). The positive X-COL axis represents the frontal zone. Higher values of Volume index in this zone indicate major probability of heavy rainfalls



c



d

Fig. 13 (continued)

COLs reach their mature state (maximum activity), as measured by higher index values. Thus, heavy rainfall events are more likely to occur during the second stage, in the frontal zone of a COL.

An important difference between cold and warm season COLs was found. Figure 13e and f

presents volume index values versus X-COL coordinates for each case in both seasons. During the cold season, volume index values for DCC are usually higher. Unless more cases of COL occurrences were chosen during warm season, as Fig. 1b shows, heavy rainfall events associated with COL

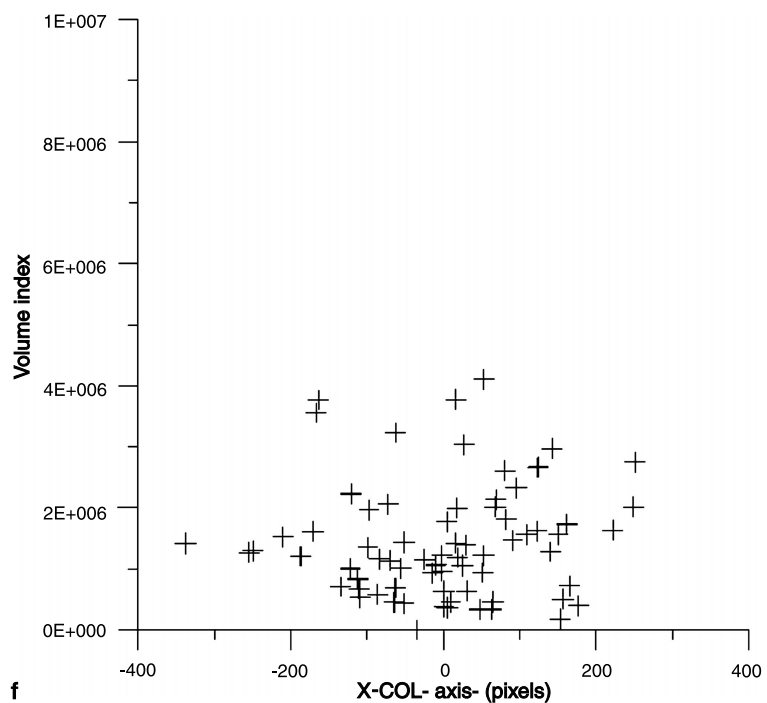
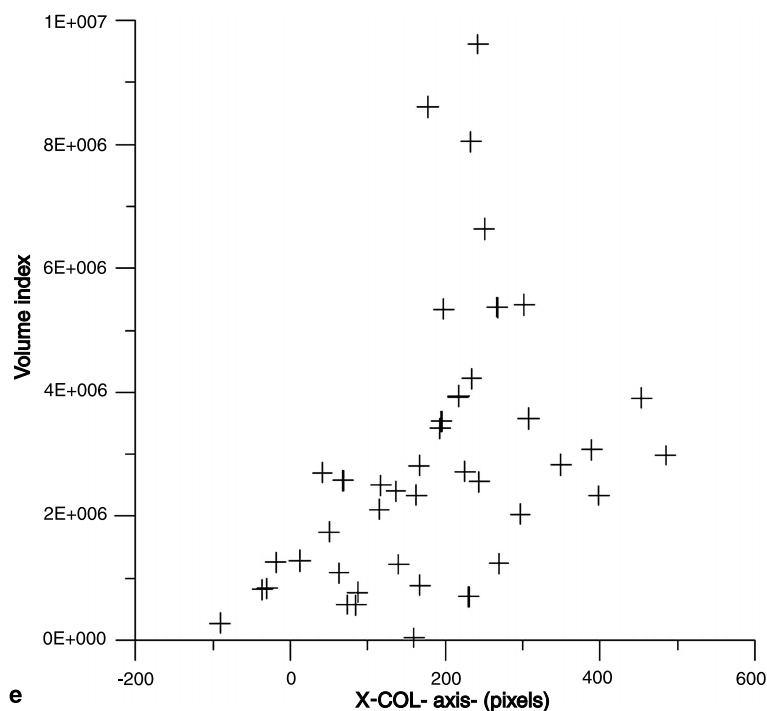


Fig. 13 (continued)

systems are more likely to occur during cold season. This result seems logical if we pay attention in the fact that the colder the pixels are, the higher the volume index is.

4. Conclusions

A cloud cover analysis of cut-off low pressure systems using a pattern recognition method ap-

plied to IR-VIS bispectral histograms was carried out in this study. 35 COL occurrences were studied over five years (1994–1998). Five cloud types were identified in COL systems, with high clouds (cirrus and cirrostratus) and deep convective clouds found to be those that better characterized COLs.

Cloud cover in COL systems is highly dependent on the stage of its life cycle, but a higher

percentage of cloud cover is always present in the frontal zone, due to higher concentrations of high clouds and deep convective clouds. The frontal zone is also characterized as being more active, with cloud top temperatures of high and deep convective cloud lower than in the rearward zone. These general characteristics are particularly striking during the upper-level trough and the tear-off. Closed cyclonic circulation at 200 hPa begins during the cut-off, minimizing differences between rearward and frontal zones.

The upper-level trough is characterized by fibrous and rough high clouds and deep convective clouds in the rearward zone and a higher presence of these clouds in the frontal zone. During the tear-off, differences in cloudiness between the two zones increase as a result of deep convection in the frontal zone. The COL reaches its mature state in this stage and the probability of heavy rains in the frontal zone is greater than in the first stage. The cut-off is characterized by the uniform distribution of cloudiness in the COL selected area, reducing differences between rearward and frontal zones. The probability of heavy rains during the third stage decreases considerably. Centres of gravity of high and deep convective cloud move to the COL-axes centre during COL evolution.

Differences in cloudiness between rearward and frontal zones are accentuated in the cold season. Clouds are also found further from the COL-axis centre and the probability of heavy precipitation in the frontal zone is significantly higher.

Acknowledgements

This work was supported by the Spanish Ministry of Science and Technology (MCYT), under grant REN2002-04558-C04-04.

References

- Arking A, Childs JD (1985) Retrieval of cloud cover parameters from multispectral satellite images. *J Climate Appl Meteorol* 24: 322–333
- Arnaud Y, Desbois M, Maizi J (1992) Automatic tracking and characterization of African convective systems on Meteosat pictures. *J Appl Meteorol* 31: 443–453
- Bamber DJ, Healey PGW, Jones BMR, Penkett SA, Tuck AF, Vaughan G (1984) Vertical profiles of tropospheric

- gases: chemical consequences of stratospheric intrusions. *Atmos Environ* 18: 1759–1766
- Desbois M, Seze G, Szejwach G (1982) Automatic classification of clouds on Meteosat imagery: application to high-level clouds. *J Appl Meteorol* 21: 401–412
- England CF, Hunt GE (1985) A bispectral method for automatic determination of parameters for use in imaging satellite retrievals. *Int J Remote Sens* 6(9): 1545–1553
- Feidas H, Cartalis C (2001) Monitoring mesoscale convective cloud systems associated with heavy storms with the use of Meteosat imagery. *J Appl Meteorol* 40: 491–512
- Feidas H, Cartalis C (2005) Application of an automated cloud-tracking algorithm on satellite imagery for tracking and monitoring small mesoscale convective cloud systems. *Int J Remote Sens* 26(8): 1677–1698
- García-Herrera R, Puyol DG, Martín EH, Presa LG, Rodríguez PR (2001) Influence of the North Atlantic oscillation on the Canary Islands precipitation. *J Climate* 14: 889–903
- Gimeno L, Hernández E, Rúa A, García R (1998) Surface ozone in Spain. *Chemosphere* 38: 3061–3074
- Hernández A (1999) Un Estudio Estadístico sobre Depresiones Aisladas en Niveles Altos (DANAs) en el Sudoeste de Europa basado en Mapas Isentrópicos de Verticidad Potencial. IV Simposio Nacional de Predicción, Instituto Nacional de Meteorología, Serie Monogr, No SM 351, Ministerio de Medio Ambiente, 235 pp
- Holton J, Haynes P, McIntyre M, Douglass A, Rood R, Pfister L (1995) Stratosphere-troposphere exchange. *Rev Geophys* 33: 403–439
- Hoskins BJ, McIntyre ME, Robertson AW (1985) On the use and significance of isentropic potential vorticity maps. *Quart J Roy Meteor Soc* 111: 877–946; Corrigendum 113: 402–404
- Kentarchos AS, Davies TD (1998) A climatology of cut-off lows at 200 hPa in the Northern Hemisphere, 1990–1994. *Int J Climatol* 18: 379–390
- Krennert T, Zwatz-Meise V (2002) Manual of synoptic satellite meteorology: conceptual models. Version 4.0, 3 CD-ROMs available at ZAMG (Austrian Meteorological Service, Hohe Warte 38, 1190 Wien, Austria)
- Llasat MC (1991) Gota fría. Boixareu Universitaria, 165 pp
- Massons J, Domingo D, Grau J (1996) Automatic classification of VIS-IR Meteosat Images. *Comp Geosci* 22: 1137–1146
- Massons J, Domingo D, Lorente J (1998) Seasonal cycle of cloud cover analyzed using Meteosat satellite images. *Ann Geophys* 16(3): 331–341
- Nieto R, Gimeno L, de la Torre L, Ribera P, Gallego D, García-Herrera R, Núñez M, Redaño A, Lorente J (2005) Climatological features of cut-off low systems in the Northern Hemisphere. *J Climate* 18(16): 3085–3103
- Pankiewicz GS (1995) Pattern recognition techniques for identification of cloud and cloud systems. *Meteor Appl* 2: 257–271

- Porcú F, Levizzani V (1992) Cloud classification using METEOSAT VIS-IR imagery. *Int J Remote Sens* 13: 893–909
- Price JD, Vaughan G (1992) Statistical studies of cut-off low systems. *Ann Geophys* 10: 96–102
- Rossow WB, Garder LC (1993) Cloud detection using satellite measurements of infrared and visible radiances for ISCCP. *J Climate* 6(12): 2341–2369
- Sèze G, Desbois M (1987) Cloud cover analysis from satellite imagery using spatial and temporal characteristics of the data. *J Climate Appl Meteor* 26: 287–303
- Wirth V (1995) Diabatic heating in an axisymmetric cut-off cyclone and related stratosphere-troposphere exchange. *Quart J Roy Meteor Soc* 121: 127–147

Corresponding author's address: Angel Redaño, Departament D'Astronomia i Meteorologia, Universitat de Barcelona, Avda. Diagonal 647, 08028 Barcelona, Spain (E-mail: angel@am.ub.es)